Molecular Architecture of the Thylakoid Membrane: Lipid Diffusion Space for Plastoquinone

H. Kirchhoff,*,‖ U. Mukherjee,‖ and H.-J. Galla§

Institut für Botanik, Schlossgarten 3, D-48149 Münster, Germany, and Institut für Biochemie, Wilhelm-Klemm-Strasse 2, D-48149 Münster, Germany

Received August 13, 2001; Revised Manuscript Received January 7, 2002

ABSTRACT: We have determined the stoichiometric composition of membrane components (lipids and proteins) in spinach thylakoids and have derived the molecular area occupied by these components. From this analysis, the lipid phase diffusion space, the fraction of lipids located in the first protein solvation shell (boundary lipids), and the plastoquinone (PQ) concentration are derived. On the basis of these stoichiometric data, we have analyzed the motion of PQ between photosystem (PS) II and cytochrome (cyt.) bf complexes in this highly protein obstructed membrane (protein area about 70%) using percolation theory. This analysis reveals an inefficient diffusion process. We propose that distinct structural features of the thylakoid membrane (grana formation, microdomains) could help to minimize these inefficiencies and ensure a non-rate limiting PQ diffusion process. A large amount of published evidence supports the idea that higher protein associations exist, especially in grana thylakoids. From the quantification of the boundary lipid fraction (about 60%), we conclude that protein complexes involved in these associations should be spaced by lipids. Lipid-spaced protein aggregations in thylakoids are qualitatively different to previously characterized associations (multisubunit complexes, supercomplexes). We derive a hierarchy of protein and lipid interactions in the thylakoid membrane.

Photosynthetic energy transduction in higher plants is coupled to the thylakoid membrane inside the chloroplast. A unique property of this membrane is the formation of stacks (grana) interconnected by unstacked stoma lamellae. Photosynthetic electron flux from water to NADP is managed by the multisubunit complexes photosystem (PS)[1] II, the cytochrome (cyt.) bf complex, PSI and ferredoxin-NADP oxidoreductase (FNR). Small diffusable electron carriers connect these protein complexes: PQ between PSII and the cyt.bf complex, plastocyanin between the cyt.bf complex, and PSI and ferredoxin between PSI and FNR. The process of light absorption and transmission of excitons to the reaction centers of PSII and PSI is performed by core antenna directly bound to the photosystems and tightly or more loosely bound light harvesting pigment−protein complexes (LHC).

In the last two decades, a number of experiments have shown that multisubunit complexes can associate to produce higher aggregation forms. These constitute homo- or heterooligomeric assemblies. Homooligomeric protein assemblies have been reported for LHCII ($LHCII_3$) (*1*, *2*) and the cyt.bf complex ($cyt.bf_2$) (*3*), while, on the other hand, heterooligomeric associations exist for the majority of photosystem II, PSIIα, $(PSII\alpha\text{-}(LHCII)_3)_2$ (*4*), and photosystem I ($PSI\text{-}(LHCI)_8$) (*1*, *5*). In contrast, it seems that another PSII type, PSII*β* center, as well as the ATPase do not form higher aggregation states. The functional role of these assemblies has not been elucidated. They may enhance the effectiveness of energy transduction in the photosynthetic process or may stabilize proteins. Here, to distinguish such associations from the multisubunit complexes we call them "supercomplexes". Analysis using electron microscopic and electron diffraction techniques on isolated complexes have provided us with a complete set of structures with a resolution of at least 2.5 nm (*2*, *4*−*7*). This data set will be applied in this study.

In addition to supercomplexes, recent evidence supports the existence of an even higher level of protein assemblies, located mainly in the grana region. (i) By fast solubilization of grana stacks, followed by electron microscopic single particle analysis, heptameric LHCII-trimers (*8*) as well as complexes formed by $LHCII_3$ and $(PSII\alpha\text{-}LHCII_3)_2$ supercomplexes (*9*) are isolated. The authors conclude that these aggregates also exist in the native membrane. (ii) The most likely explanation for the well-established phenomena of energy-transfer between PSIIα units (cooperativity) (*10*) is that several PSIIα centers share a common antenna bed mediated by LHCII complexes. To facilitate energy transfer, close contact between several of these complexes must occur. (iii) Analysis of light-induced changes in circular dichroism of thylakoids indicates the existence of a long-range chiral order. These signals are interpreted as indicating a macrodomain structure in grana stacks (*11*). (iv) Associations between a fraction of PSI centers and $LHCII_3$ located in the

* To whom correspondence should be addressed. Phone: +49 251 8324820; fax: +49 251 8323823; e-mail: kirchhh@uni-muenster.de.
‖ Institut für Botanik.
§ Institut für Biochemie.

[1] Abbreviations: chl, chlorophyll; cyt, cytochrome; DCMU, 3-(3,4-dichlorophenyl)-1,1-dimethylurea; DGDG, digalactosyl diacylglycerol; HEPES, *N*-2-hydroxyethylpiperazine-*N*′-2-ethane-sulfonic acid; LHC, light harvesting complex; MGDG, monogalactosyl diacylglycerol; PC, phosphatidylcholine; PG, phosphatidylglycerol; PQ, plastoquinone; PS, photosystem; SQDG, sulfoquinovosyl diacylglycerol.

10.1021/bi011650y CCC: $22.00
Published on Web 03/20/2002

grana margins are postulated (*12*, *13*). (v) From a functional analysis of electron transport reactions, a microdomain hypothesis was developed originally postulated by Joliot, Lavergne, and co-workers (*14*, *15*) and extended by others (*16*, *17*). According to the microdomain hypothesis, $(PSII\alpha\text{-}LHCII_3)_2$ and $LHCII_3$ build up a network-like arrangement, within which plastoquinone molecules are temporarily trapped. The participation of cyt.bf complexes in these networks is unclear. In contrast to supercomplexes, it is expected that microdomains are less stable structures with a finite lifetime (*17*, *18*).

Given their existence, it is an open question as to whether microdomains are random (*15*) or more ordered structures resulting from specific protein interactions (*17*). In either case, significant influences on the plastoquinone diffusion process are expected. From the viewpoint of a plastoquinone molecule, the thylakoid membrane is highly obstructed, by integral proteins, which are visualized in electron micrographs of freeze-fractured membranes (*19*, *20*). From these images, the intuitive question arises, is an efficient diffusion process still possible in such a crowded membrane? The efficiency of PQ diffusion is a critical factor, since dissipation of energy by inefficient diffusion would decrease the overall quantum yield for energy transduction (*21*). Furthermore, an over-reduction of the plastoquinone pool could occur, which would trigger acceptor side photoinhibition of photosystem II (*22*). In this context, the role of microdomains remains elusive. Such structures would prevent long range diffusion between grana stacks and stroma lamellae, making this electron transport inefficient. As a consequence, only cytochrome bf complexes located near to active PSII complexes in grana regions would have good access to reduced PQ. This scenario would provide a mechanistic explanation for the idea that linear electron transport is restricted only to grana thylakoids (*23*, *24*). The restriction of long range PQ movement does not automatically imply that short-range diffusion within appressed membranes is also inefficient. Here, we demonstrate that short-range diffusion in a hypothetical membrane with a random protein distribution and a protein density determined from our stoichiometric analysis is inefficient. In this context, we discuss advantages of grana formation and microdomains for the process of short-range plastoquinone diffusion.

While there is good evidence for the existence of higher-level protein associations, especially in grana thylakoids, almost nothing is known about the involvement of lipids in these associations. In particular, an important question is whether supercomplexes arranged in higher associations are spaced by lipids or not. In principle, the membrane embedded parts of proteins could form stable associations either with other proteins or with lipids. It is likely that direct protein−protein contact leads to more stable structures than protein−lipid−protein associations.

Thus, the involvement of lipids in supercomplex associations would influence the flexibility of these structures. This could be important for dynamic adjustments of the photosynthetic apparatus in response to changing environmental conditions. In this study, we examine the involvement of lipids between supercomplex associations by calculating the fraction of boundary lipids located in the first solvatiation shell of membrane integral proteins.

Furthermore, we deduce the photochemically active plastoquinone concentration in the thylakoid membrane. Two pools of plastoquinone can be distinguished in chloroplasts. In addition to a functional active pool involved in photosynthetic electron transport, an inactive pool exists, localized in plastoglobuli. The knowledge of the active plastoquinone concentration in thylakoid membranes (given in moles per liter) is a prerequisite for considering several questions concerning the photosynthetic electron transport. This parameter is necessary for the simulation of PQ-dependent electron transport reactions (*17*, *25*) or calculations of PQ-binding constants from the kinetic and thermodynamic properties of redox centers (*26*). A number of publications give *relative* plastoquinone concentration values (in moles per moles). These data refer the plastoquinone content to the content of other components of the thylakoid membrane including chlorophyll (*27*), lipids (*27*), or photosystem II (*10*). To our knowledge, there has so far only been one *absolute* value quoted (*16*), while other values are deduced from theoretical considerations (*25*, *26*).

MATERIAL AND METHODS

Thylakoid Preparation. Spinach leaves from 6−8-week-old plants (*Spinacea olearacea* var. polka), grown in a hydroculture medium (*28*) at 13 to 16 °C with 10 h daylength (about 300 μmol of quanta m^{-2} s^{-1}), were harvested and washed. The leaves were ground in a medium containing 330 mM sorbitol, 0.5 mM KH_2PO_4, 50 mM KCl, 1 mM $MgCl_2$, 1 mM $MnCl_2$, 2 mM EDTA, and 25 mM MES (pH 6.1). The homogenate was filtered and centrifuged at 2000*g* for 1 min. The pellet was resuspended in a medium containing 5 mM $MgCl_2$, 150 mM NaCl, and 20 mM Tricine (pH 7.8) and centrifuged. After a washing step, thylakoids were resuspended in a medium containing 7 mM $MgCl_2$, 10 mM KCl, 330 mM sorbitol, and 50 mM HEPES (pH 7.5). Chlorophyll concentrations were determined according to ref *29*. The suspension was aliquotated, flash frozen, and stored at −70 °C in the dark.

Quantification of Thylakoid Lipid Components. All steps for the lipid analysis were done in a N_2 atmosphere to minimize the contact with oxygen. For the isolation of lipids, 1 mL of 2-propanol was added to 1 mL of thylakoid suspension (adjusted to 0.5 mg of chlorophyll/mL), heated to about 95 °C for 10 min, cooled, and mixed with 12 mL of chloroform/methanol (2:1) and then with 3.5 mL of 0.9% aqueous KCl solution. After centrifugation (5 min 1000*g*), the lower phase was quantitatively harvested, and the organic solvents were evaporated under N_2 gas. The dried lipids were suspended in 1 mL of chloroform and stored at −20 °C (lipid extract).

The separation and quantification of the individual lipids were carried out using thin-layer chromatography on precoated silica gel 60 plates (Merck, Germany), as described in ref *30*. Prior to this, the exact chlorophyll concentration of the lipid extract was determined. A 300 μL lipid solution was applied to an activated (30 min 130 °C) chromatography plate. The solvent system for the separation consisted of chloroform/methanol/H_2O in a ratio of 65:25:2. Lipid bands were visualized using iodine vapor and marked. Iodine was evaporated (15 min 130 °C), and the marked bands were scraped off for quantification. For the identification of the individual bands, see Results. The galactolipids were quantified spectroscopically according to ref *31*. Phospholipids

were quantified by the ammonium molybdat method according to ref *32*.

Surface-Pressure Area Isotherms. Surface-pressure area isotherms were measured with a computer supported film balance from NIMA Technology (type 601M, Coventry, UK). A total of 6.9 or 8.3 nmol of a thylakoid lipid mixture dissolved in chloroform was spread on the water-filled (Milli-Q quality) Teflon trough (area 91 cm^2). The surface pressure was detected with a Wilhelmy plate system. After evaporation of chloroform, the compression and expansion of the monolayer were done with a barrier speed of 5 cm^2/min. The film balance was temperature controlled to 20 ± 0.1 °C.

Spectroscopy. Quantitative absorbance changes (Δabs) of particular marker redox centers were measured for the quantification of PSI (P700), PSII (C550 signal), and cytochrome bf complex (cytochrome f and b_6). For P700 and C550 determination, thylakoids were incubated for at least 5 min in a medium containing 80 mM KCl, 7 mM $MgCl_2$, 300 mM sorbitol, 30 mM HEPES (pH 7.6), 0.2% (w/v) β-dodecylmaltoside. Additionally, 10 μM methyl viologen and 5 mM sodium ascorbate were added for P700 or 6 mM ferricyanide and 10 μM DCMU for C550. The experimental setup was as described previously (*17*). Saturating light pulses of 50 ms were given to induce quantitative redox changes. The concentration of the cytochrome bf complex was determined from chemically induced absorbance changes. Thylakoids were incubated in 20 mM KCl, 50 μM EDTA, 20 mM HEPES (pH 7.6), and 0.03% (w/v) β-dodecylmaltoside. Stepwise redox changes were induced by addition of 1 mM ferricyanide, 5 mM sodium ascorbate, and small grains of sodium dithionite. Absorbance changes in the range of 520 to 580 nm were recorded using a Hitachi U3010 photometer with a head on photomultiplier. The spectra were fitted with reference spectra for cytochrome f, high potential cytochrome b559 and P700 (ascorbate minus ferricyanide) and cytochrome b6, low potential cytochrome b559 and C550 (dithionite minus ferricyanide). The reference spectra were taken from refs *17* and *33*. Differential extinction coefficients for cytochrome f were taken from ref *34* and for cytochrome b6 from ref *35*. Before curve fitting, a baseline was subtracted, defined by the wavelengths 540 and 575 nm. The baseline corrected coefficients are 28.7 and 22.0 mM^{-1} cm^{-1} for cytochrome f and b6, respectively.

From the maximum absorbance changes, the concentrations of the redox centers were calculated using eq 1 (*36*).

$$c = \frac{\Delta\text{abs}}{\Delta\epsilon d} \quad (1)$$

where c is the concentration of the component in mM, d is the optical path length of the cuvette (1.75 cm), Δabs is the maximal absorbance change, and $\Delta\epsilon$ is the differential extinction coefficient in mM^{-1} cm^{-1} at a given wavelength or wavelength pair, respectively.

The determination of PSII by C550 measurement is based on the method described in ref *37* with a differential extinction coefficient of 3.6 mM^{-1} cm^{-1} deduced from ref *38*. The differential extinction coefficient for P700 is taken from ref *39*.

Chlorophyll-*a* fluorescence induction curves were recorded from thylakoids (10 μg/mL chlorophyll) incubated in the same medium as for P700 and C550 measurements. Additionally, 10 μM DCMU and 1 μM nigericin were present. The experimental setup was as described in ref *17*. Before induction measurements, the samples were incubated for at least 10 min in the dark at 7 °C.

Quantification of Light Harvesting Complexes. The LHCII content of thylakoids was derived from a quantification of the Coomassie R250 brilliant blue staining of SDS/PAGE gels according to ref *40*. This method is based on the comparison of the stain intensity of LHCII bands from the sample with the stain intensity of the bands from purified protein on the same gel. LHCII isolated from pea was a kind gift of M. Lamborghini, Frankfurt a.M., Germany. A 16.5% acrylamide spacer gel was used, and the LHCII content was quantified from a scanner analysis (AGFA photo look software), using the program OPTIMAS, version 5.1. For the determination of the LHCII content by this method, it is important to note that Lhca3 proteins (24 kDa) associated with PSI (*1*) could run at the same position as LHCII proteins (V. H. R. Schmid, Mainz, Germany, personal communication). Therefore, the LHCII content derived from the quantification of the gel bands are corrected by double the concentration of photosystem I, because each PSI binds two Lhca3 gene products (*1*).

Quantification of ATPase. The ATPase content was determined from quantitative analysis of stained SDS gel bands using the CF1 protein from the ATPase, as described in ref *41*. The method involves detachment of the CF1 part from washed thylakoids by a NaSCN treatment (30 s, 2 M). After centrifugation (4 min, full speed Beckmann microfuge E) of the sample, the proteins in the supernatant were precipitated using 1 M TCA, on ice. The denaturated proteins were pelleted, separated by SDS gel electrophoresis, stained with Coomassie Brilliant Blue, and destained as described in ref *41*. Staining of the separated α- and β- subunits of the CF1 part was estimated by comparison with isolated reference proteins (a kind gift of Dr. Strotmann, Düsseldorf, Germany) and used for calculation of the CF1 concentration (*41*).

RESULTS

Lipid Analysis. (1) Determination of Lipid Content by Thin-Layer Chromatography. Figure 1 shows an example of the separation of thylakoid lipids achieved by thin-layer chromatography. Lipids were visualized using iodine vapor. The assignment of a particular band to a lipid class was carried out in two ways. First, MGDG, DGDG, and PG were identified by comparison with reference lipids (Sigma) run in parallel to the thylakoid lipids. Second, the galactolipid SQDG was assigned by staining with α-naphthol and the phospholipids with a molybdate spray (*42*), resulting in brownish and blue color, respectively. The correctness of these assignments are supported by comparison with thin-layer chromatography plates running under similar conditions (*30*). The quantification of the lipid content, expressed relative to the amount of chlorophyll, is summarized in Table 1 (left-hand column).

The relative distribution of the lipid classes, as well as the total number of lipids per chlorophyll, agrees well with published values (*43*−*45*). It was found that pure thylakoid membranes contain no PC (*46*). The appearance of this lipid

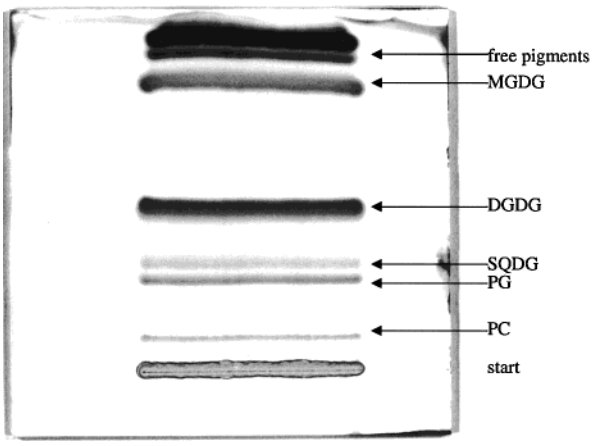

FIGURE 1: Thin-layer chromatography of a thylakoid lipid extract. Lipid bands were visualized using iodine vapor, giving a brownish color. The free pigment bands were yellow (lower bands) and green (upper bands), and the starting band was colorless. For the identification of particular bands, see text.

Table 1: Lipid Content of the Thylakoid Membrane[a]

lipid	mol of lipid/ mol of chlorophyll	correction for envelope membranes mol of lipid/ mol of chlorophyll
MGDG	1.04 ± 0.05	0.84 ± 0.07
DGDG	0.70 ± 0.03	0.51 ± 0.05
SQDG	0.42 ± 0.02	0.38 ± 0.02
PG	0.28 ± 0.01	0.22 ± 0.01
PC	0.13 ± 0.01	
Total	2.57 ± 0.12	1.95 ± 0.15

[a] Values from three independent determinations. The correction (right column) is based on the fact that pure thylakoid membranes contain no PC (see text).

species in our thylakoid preparation can be put down to contamination by the outer envelope membrane. Provided that the individual ratio of PC to the other lipid classes given in Table 1 for pure total (outer + inner) envelope membranes is known, it is possible to calculate the amount of lipids coming from the envelope and to correct the measured values (*46*). The result of this correction is given in the right column and is based on the following ratio for envelope membranes: MGDG/DGDG/SQDG/PG/PC = 1.60:1.50:0.30:0.45:1 (*46*).

(2) Surface-Pressure Molecular Area Isotherms of a Native Thylakoid Lipid Mixture. We deduced the molecular area covered by thylakoid lipids from surface-pressure area isotherms. These measurements were performed with a mixture of single lipids isolated from thylakoids by thin-layer chromatography. Figure 2 shows a surface-pressure area isotherm measured with a monolayer of this thylakoid lipid mixture. Three compression/expansion cycles of the monolayer film are depicted. In an independent experiment, we found that the monolayer collapses at a surface pressure of about 45 mN/m (horizontal dashed line in Figure 2). On the basis of this value, we decide to restrict the maximal surface pressure to 40 mN/m in the repetitive compression/expansion experiment. Obviously, the monolayer film in the first cycle shows a higher compressibility and higher molecular areas than in the second and third cycles. This phenomenon is often observed in this kind of experiment and can indicate a rearrangement of the lipid mixture during the first compression, due to disorder from the spreading process. To generate an equilibrium state of the monolayer, which is comparable to conditions within a bilayer of thylakoid lipids, the monolayer was compressed and expanded one time to exclude artifacts from the spreading process. Thus, we take the second and third compression isotherms to calculate the molecular area of the thylakoid lipid mixture.

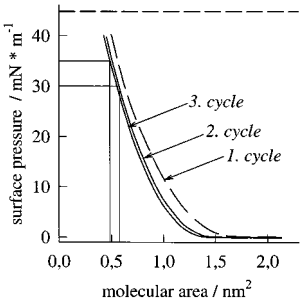

FIGURE 2: Surface-pressure molecular area isotherm of a native thylakoid lipid mixture. Three compressions with one lipid mixture are depicted. After compression and decompression, another cycle begins at zero surface pressure. For clarity, the decompression curves are omitted. A lipid volume corresponding to 6.9 or 8.3 nmol lipid mixture was put on the water surface of the film balance. Both amounts gave identical results. The composition and concentration of the lipid mixture, measured by thin-layer chromatography, results in a ratio of MGDG/DGDG/SQDG/PG/PC of 0.52:0.27:0.15:0.03:0.03. The horizontal dashed line indicates the surface-pressure where the lipid monolayer film begins to collapse (about 45 mN/m), as determined in an independent measurement. Thin lines indicate 30 and 35 mN/m surface-pressure (horizontal), which were used to derive the average molecular area (vertical lines) of the lipid mixture. The curves are the average of three independent measurements.

The internal lateral surface pressure in biological membranes is mainly governed by hydrophobic forces (*47*). From both theoretical thermodynamic considerations and experimental results, a surface pressure of 30 to 35 mN/m is deduced (*47*). The reliability of this range is supported by the fact that it is deduced from different methods. One argument is that activities of membrane integral proteins incorporated in artificial bilayers are comparable with in vivo activities only when the surface pressure is in the above-mentioned range (*47*). Furthermore, different membrane bilayer properties, such as transition temperature shift, enzyme turnover numbers, partition coefficient, etc. measured on monolayers, as a function of surface pressure, are observed at pressure values of 30 to 35 mN/m (summarized in ref *47*). For these values, a span for the average molecular area of thylakoid lipids from 0.49 nm^2 (35 mN/m third cycle) to 0.58 nm^2 (30 mN/m second cycle) can be deduced from Figure 2. It is notable that this represents an average lipid occupation area. This area is given by the weight areas of the individual thylakoid lipids listed in Table 1. By determining the average area of a lipid mixture, rather than of individual lipid species, possible interactions and packing effects between distinct lipids are considered.

Stoichiometric Analysis of Membrane Protein Complexes. The photosystem I and II content of thylakoid membranes was determined from light pulse induced difference absorbance signals shown in Figure 3A,B. The content of cytochrome bf complexes in thylakoids was estimated from chemical difference absorbance signals of the cytochromes. The difference signals shown in Figure 3C are fitted with

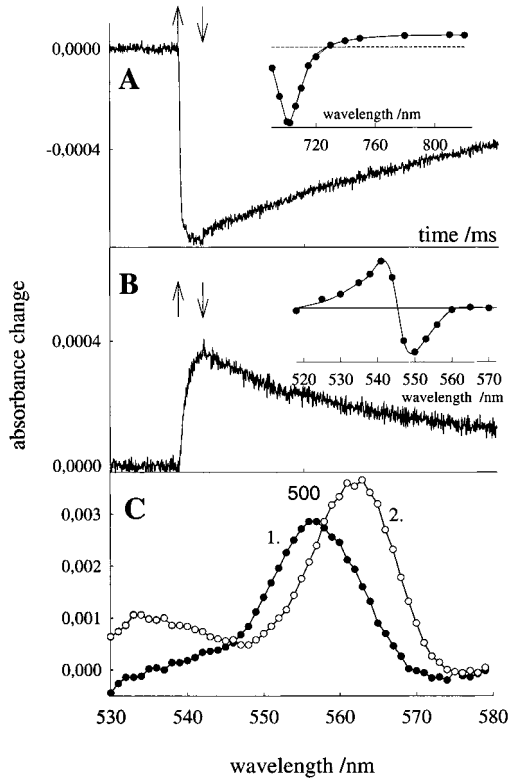

FIGURE 3: Light pulse-induced absorbance difference signals of P700 (A) and C550 (B). Arrows indicate light pulse on (upward) and off (downward). For each measurement, the chlorophyll concentration in the cuvette was precisely determined (P700, 6.85 or 7.03 μM; C550, 37.05 or 37.98 μM). The curves were derived from averaged signals: 20 measurements at 702 nm for P700 and 15 measurements at 540 and 550 nm for C550, respectively. The repetition frequency was 0.09 Hz. For the P700 signal, a fluorescence artifact was subtracted. The C550 signal is the difference of absorbance changes at 540 and 550 nm. Light pulses had an intensity of about 6000 μmol quanta m^{-2} s^{-1}. The insets show reference spectra determined for the given measuring conditions. They are in good agreement with published spectra of isolated protein complexes (*39*) for P700, (*88*) for C550. (C) Chemically induced difference absorbance signals for cytochrome bf determination. The chlorophyll concentration is 41.28 or 39.54 μM. 1. Sodium ascorbate minus ferricyanide difference spectrum. This spectrum was fitted with cytochrome f, cytochrome b559 high potential and P700. 2. Sodium dithionite minus sodium ascorbate difference spectrum, fitted with cytochrome b6, cytochrome b559 low potential and C550.

cytochrome f, cytochrome b559 high potential and P700 (ascorbate minus ferricyanide) and cytochrome b6, cytochrome b559 low potential, and C550 reference spectra as described in the methods. The values determined for PSI, PSII, and cytochrome bf complex are summarized in Table 2. These lie within the range of published values (*48*−*50*). It is notable that the concentration of protein complexes in thylakoids is not a fixed quantity but depends on genetic and environmental conditions.

(1) Light Harvesting Complexes. Figure 4 shows the SDS/PAGE gel used for LHCII quantification. It can be seen that the resolution is high enough to distinguish between 25 and 24 kDa bands. For quantification, we analyzed both bands, giving an LHCII concentration of 33.68 ± 0.76 mmol/mol of chlorophyll.

(2) ATPase. ATPase concentration was determined by quantitative SDS gel electrophoresis of stroma-side extrinsic protein components from washed thylakoids (*41*). The

Table 2: Content of Multisubunit Complexes in the Thylakoid Membrane[a]

component	mmol/mol of chlorophyll
PSI	2.25 ± 0.17
PSII	2.99 ± 0.22
cyt.bf complex	1.29 ± 0.05
LHC II	33.68 ± 0.76
ATPase	0.95 ± 0.06

[a] The values are determined from the same preparation as for lipid quantification. The ATPase determination is derived from a different membrane preparation. Values are the mean of 2 to 4 independent experiments.

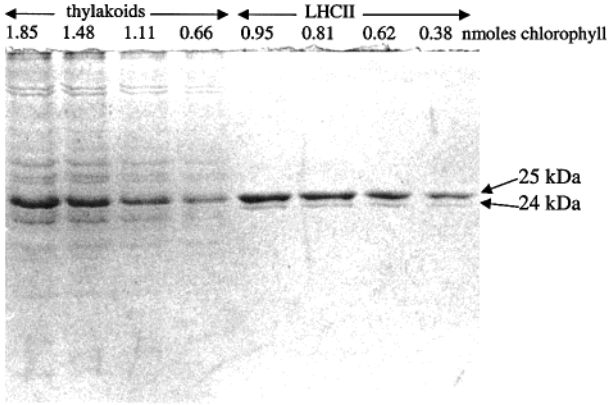

FIGURE 4: SDS−PAGE analysis for LHCII quantification of thylakoid membranes. The stain intensity of the bands from isolated LHCII (right lanes) was used to determine the LHCII content of thylakoids. For further details, see text.

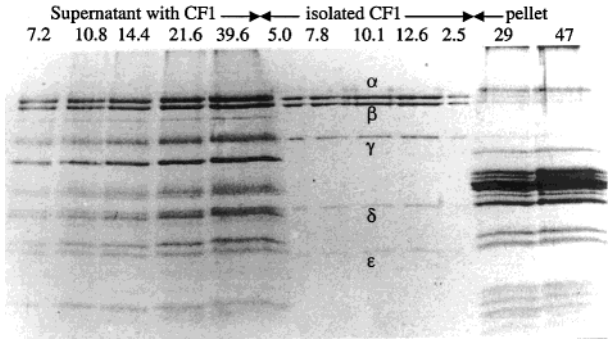

FIGURE 5: SDS−PAGE analysis for CF1 quantification of thylakoid membranes. The supernatant (left block, containing CF1) and the pellet (right block) of NaSCN treated thylakoids are depicted. In the middle block, a CF1 standard from isolated ATPase was loaded onto the gel. The numbers indicate nmol of chlorophyll for thylakoids and pmol of CF1 for the standard. Greek letters indicate the CF1 subunits. The α- and β-bands were cut out and quantified by comparing the coloring with the CF1 standard bands. A blank of the gel background was subtracted, in each case. Molecular weights for CF1 subunits are 54.8 kDa (α), 53.7 kDa (β), 35.8 kDa (γ), 20.5 kDa (δ), and 14.7 kDa (ϵ). Note that the CF1 bands occur in the supernatant and are largely absent in the pellet, indicating a quantitative removal of the CF1 from thylakoid membranes.

extrinsic protein components were extracted from thylakoids by NaSCN treatment (*41*). Figure 5 shows that this treatment removes the CF1 subunits of the ATPase complex from the thylakoid membrane. The concentrations of the α- and β-subunits of CF1 were determined spectroscopically at 596 nm after cutting out the gel bands and dissolving them in chloroform, by comparison with the CF1 standard (see Figure 5). From this analysis, we calculate a value of 0.95 mmol of

Table 3: Content and Area of Protein Supercomplexes in the Thylakoid Membrane[a]

supercomplex	area per complex nm^2	conc mmol/ mol of chl.	total area nm^2/chl.
PSI-LHCI$_8$	189.7	2.25 ± 0.17	0.43 ± 0.03
(PSIIα-LHCII$_3$)$_2$	285.2	1.09 ± 0.08	0.31 ± 0.02
PSIIβ[b]	108.6	0.66 ± 0.05	0.07 ± 0.01
PSIIγ[c]		0.15 ± 0.01	
LHCII$_3$	34.0	9.05 ± 0.41	0.31 ± 0.01
cyt.bf$_2$	51.3	0.65 ± 0.03	0.03 ± 0.01
ATPase	30.1	0.95 ± 0.06	0.03 ± 0.01
total		16.13 ± 1.33	1.18 ± 0.09

[a] The contours of supercomplexes were derived from the following literature: ref *4* for (PSIIα-LHCII$_3$)$_2$, ref *2* for LHCII$_3$, ref *87* for PSI-LHCI$_8$, ref *7* for cytochrome bf$_2$, ref *6* for the CFo part of the ATPase. [b] The area for PSIIβ is derived from the (PSIIα-LHCII$_3$)$_2$ supercomplex, assuming that PSIIβ is a monomer without LHCII$_3$ bound. [c] The area for PSIIγ is ignored (see text). If necessary, a detergent shell of 1.7 nm is subtracted before area determination.

ATPase/mol of chlorophyll. This is in good agreement with previously published values (*41*).

(3) Composition and Shape of Protein Supercomplexes. As mentioned in the introduction, there is good evidence for many multisubunit complexes in thylakoid membranes that are organized in noncovalently linked homo- or hetero-oligomers, termed supercomplexes. The composition and molecular area of the supercomplexes are deduced from the literature and are summarized in Table 3.

(a) PSI-LHCI$_8$. The structural organization state of higher plant PSI is monomeric. Particles can be isolated where a PSI complex is surrounded by a ring of eight monomeric LHCI proteins (*5*). It is very likely that this PSI-LHCI$_8$ assembly occurs also in vivo since the calculated antenna size of about 210 chlorophyll's per reaction center agrees well with measured values (*51*).

(b) PSII-LHCII$_3$ Dimer. It is widely accepted that PSIIα centers localized in the grana region are in a dimeric state, with one relatively strongly bound LHCII trimer per reaction center, forming a (PSIIα-LHCII$_3$)$_2$ supercomplex (*4*). While the localization of PSIIβ remains controversial, there is no doubt as to its monomeric state (*52*). As PSIIβ centers have a 2 to 3 times smaller antenna size than PSIIα, it is reasonable to assume that they have no LHCII bound. This is supported by biochemical analysis, indicating that agranal PSII binds all minor antenna complexes but no LHCII (*53*). On the basis of these data, we have calculated the area of PSIIβ centers from the (PSIIα-LHCII$_3$)$_2$ complex (see Table 3). Recently, a third type of PSII center, called PSIIγ, was detected (*54*). The concentration of this center is very low, and there are results indicating a diminished trapping efficiency (*52*). We quantified the relative amount of these different PSII centers from chlorophyll-*a* induction curves measured with DCMU-poisoned (20 μM) thylakoids (not shown). First order analysis of the normalized area growth reveals three components corresponding to the three types of centers described above. Because of the relatively low concentration of PSIIγ (max. 5%, see Table 3) and the absence of structural data, we have ignored this type of center in the following. From the total PSII concentration (Table 2) and the relative contributions for PSII subtypes, we have calculated the concentration for PSIIα and PSIIβ in the thylakoid membrane, respectively.

(c) LHCII Trimer. There is good evidence for a trimeric organization of LHCII protein in thylakoids (*1*). Structural data, with the highest resolution so far reported for thylakoid membrane proteins, are available (*2*, *55*). Table 3 shows the content of LHCII trimers not firmly bound in the (PSIIα-LHCII$_3$)$_2$ supercomplex.

(d) Cytochrome bf Complex Dimer. The cytochrome bf complex can be isolated either in a monomeric or dimeric form (*56*). There are indications that only the dimeric complex is active (*57*, *58*). Additionally, when the isolated complex is reconstituted in liposomes it forms dimers (*59*). A dimeric form is isolated from stroma lamellae and grana fragments by a combination of sonication and two-phase partitioning (*56*). The dimeric state is more established for the cyt.bc complex (*60*); however, based on the above arguments, we assume a dimeric state of the cytochrome bf complex in thylakoid membranes. The structure of the dimeric cyt.bf complex is taken from ref *7*.

(e) ATPase. So far there are no indications for a hetero- or homooligomeric assembly of the ATPase. The shape of the membrane spanning CFo part is taken from ref *6*.

On the basis of these data and with the concentrations of monomeric protein complexes (Table 2), we calculated the concentration of supercomplexes summarized in Table 3 (middle column). Additionally, the total area per chlorophyll (right-hand column) is given from the area per complex and the concentration of the complexes.

DISCUSSION

Diffusion Space for Plastoquinone in the Thylakoid Membrane. The lipid analysis results in an average molecular lipid area of 0.49 to 0.58 nm^2 (for subsequent calculations we use the mean, 0.54 ± 0.05 nm^2) and a concentration of 1.95 ± 0.15 lipids/chlorophyll. Assuming that all lipids are organized in a bilayer, a total bilipid area of 0.53 ± 0.05 nm^2/chlorophyll molecule is attained. The area of all integral proteins in the thylakoid membrane is 1.18 ± 0.09 nm^2 (Table 3). Thus, each chlorophyll molecule corresponds to a thylakoid membrane area of 1.71 ± 0.14 nm^2. It follows that 31 ± 5% of the thylakoid membrane area is occupied by lipids, while the remaining area is covered by integral proteins. A slightly higher lipid area fraction of 40% was found in earlier studies (*44*). In contrast to these studies, we incorporate in our analysis a quantification and distinct structural information on each individual protein complex and, furthermore, derive the lipid occupation area experimentally. The lipid area derived from electronmicroscopic analysis on freeze-fractured membranes is higher than in our study. From the literature (*19*), we derive values of 39 to 52% for stacked membranes and 51 to 68% for unstacked membranes. We have no definite answer to explain these discrepancies but it should be noted that plastic deformations during freeze-fracturing can reduce particle sizes (*61*). In addition, a reduction in platinum deposition on samples with high protein densities can further decrease the apparent particle size (*61*). If we calculate the lipid area from protein densities taken from freeze-fracture analysis (*19*) and the protein areas from Table 3, the lipid area fraction would be 24 to 49%, which is in agreement with our estimate. For this calculation, a ratio of stacked to unstacked membranes of 60:40 is assumed (*19*).

It is important to note that the thylakoid membrane contains free carotenoids. For different plants growing under low or high light conditions a mean value of 0.07 mol carotenoids/mol of chlorophyll (range 0.05 to 0.10) is calculated (*62*). The molecular area of violaxanthin and zeaxanthin is about 0.8 nm^2 (*63*), given a total carotenoid area of 0.06 nm^2/chlorophyll. About 60% of these carotenoids are involved in the xanthophyll cycle (*64*). It is assumed that these pigments are located at the protein boundaries (*64*). Thus, it can be estimated that about 0.04 nm^2 carotenoid/chlorophyll belong to the lipid phase. This is equivalent to less than 2% of the total membrane area. For further calculations, we neglect this component.

To examine the consequences of this protein-rich lipid area on plastoquinone diffusion, we have analyzed the diffusion process using percolation theory, based on our protein density data. Percolation theory describes the hindrance of two-dimensional diffusion of a tracer molecule (PQ) in an archipelago of obstacles (integral proteins) (*65*, *66*). The unhindered diffusion is described by Einstein's equation correlating the average of the square displacement for a tracer ($\langle r^2 \rangle$) with time (t). For a two-dimensional process the eq is

$$\langle r^2 \rangle = 4Dt \tag{2}$$

Percolation theory corrects the diffusion coefficient D for the effects of collision and trapping by obstacles, giving a new coefficient D^*. The original theory deals with immobile obstacles, which could form a finite cluster completely surrounding a diffusion space when the obstacle concentration exceeds a particular threshold (*65*). We have applied an extended version of this theory (*65*) where the obstacles themselves can move (self-diffusion). For this situation, D^* approximates asymptotically and very rapidly to a distance-independent value (*66*), which is given by eq 3 (*65*):

$$D^* = (1 - c)\frac{\sqrt{[(1-\gamma)(1-c)f_0 + c]^2 + 4\gamma(1-c)f_0^{\,2}} - (1-\gamma)(1-c)f_0 + c}{2\gamma(1-c)f_0} \tag{3}$$

with

$$f_0 = (1 - \alpha)/[1 + (2\gamma - 1)]\alpha$$

where c is the area fraction occupied by obstacles, γ is the jump rate ratio of tracer to obstacles, and α is a constant depending on the lattice geometry.

The ratio of the jump rates (γ) can be obtained from the unhindered diffusion coefficients for tracer and obstacles. For plastoquinone, a diffusion coefficient in pure liposomes of $1-3.5 \times 10^{-7}$ cm^2 s^{-1} (for further calculations we use the mean $2.3 \pm 1.3 \times 10^{-7}$ cm^2 s^{-1}) was determined (*67*, *68*). The situation for integral protein complexes in thylakoid membranes is more complicated. A value of 4.4×10^{-10} cm^2 s^{-1} has been determined for the cytochrome bc1 complex of mitochondria (*69*). In ref *70*, a microscopic diffusion coefficient for $LHCII_3$ of $2-4 \times 10^{-12}$ cm^2 s^{-1} was derived from Monte Carlo simulations. The authors concluded that this low value is because protein−protein interactions occur between $LHCII_3$ and between $LHCII_3$ and photosystem II, while these interactions are missing for the cytochrome bc1 complex. From these values, we estimate an average diffusion coefficient for our model membrane of 2×10^{-10} cm^2 s^{-1}, based on individual weighted diffusion coefficients (weight numbers from Table 3). This calculation is based on the assumption that D is proportional to the inverse of the radius of the protein complexes, and that for $(PSII\alpha\text{-}LHCII)_3)_2$ and $LHCII_3$ the lower diffusion coefficient and, for all other complexes, the upper value is valid. From these diffusion coefficients, a value of 1000 for γ is deduced. The meaning of this value is that plastoquinone requires only 1/1000 of the time to travel a given distance in a pure lipid membrane than does an average thylakoid protein. For high values of γ (> 10), D^* calculated with eq 3 is lower than that determined from Monte Carlo simulations (*65*). We resolve this problem as follows. For $\gamma \rightarrow \infty$ (strongest deviation), the predicted Monte Carlo value can easily be obtained from eq 3 if, instead of the true area fraction (c), a value of c minus 0.06 is used. We derived this value from Figure 3 in ref *65*. Thus, we calculate the D^* value for the thylakoid membrane for a protein area fraction of 0.63 instead of 0.69, given a D^* value of 0.4 to 2.5×10^{-3} depending on the lattice geometry. With the PQ diffusion coefficient for pure liposomes (see above), a corrected coefficient range of $0.9 \pm 0.2 \times 10^{-10}$ to $6.7 \pm 1.6 \times 10^{-10}$ cm^2 s^{-1} is given. For further calculations, we use the mean value $3.8 \pm 2.9 \times 10^{-10}$ cm^2 s^{-1}, which is in the range of measured values of 1 to 30×10^{-10} cm^2 s^{-1}, deduced from steady-state pyren fluorescence data (*16*).

To analyze the PQ diffusion in a membrane with the deduced protein density using percolation theory, the mean distance between PSIIα complexes and cyt.bf complexes must be known. Therefore, we calculated a random protein distribution for PSIIα and cyt.bf complexes in a 300×300 nm membrane region with the program MATHCAD, where protein overlap is avoided. We assumed a circular shape for both complexes, with diameters of 15 nm for PSIIα and 8 nm for cyt.bf. The densities of 56 $(PSII\alpha\text{-}LHCII_3)_2$ and 34 $(cyt.bf)_2$ for this area of 0.09 μm^2 were calculated from the total membrane area and the numbers in Table 3. To determine the distance from PSIIα to the closest cyt.bf complex, only PSIIα centers located in an inner square of 200×200 nm were analyzed, to avoid edge effects. We estimate an average distance of 35 nm (three independent distributions were analyzed, range 33 to 38 nm).

This value is equivalent to the average distance a PQH_2 must travel by a random walk through the protein obstructed lipid phase. With the corrected diffusion coefficient deduced from percolation theory given above, an average diffusion time of 8 ± 6 ms is predicted. If the diffusion is not restricted, the time is only about 10 μs (eq 2), which reflects the fact that the path of the plastoquinone molecule is greatly extended by a large number of collisions with proteins. Furthermore, three points not considered in percolation theory must be taken into account, which increase the apparent diffusion time of the PQH_2 molecule. First, it is unrealistic to assume that PQH_2 binding at the Qo site of the cyt.bf complex takes place at the first encounter, because no electrostatic recognition exists between the two species, as described for plastocyanin and photosystem I (*71*). Electrostatic attraction helps to build a reaction complex efficiently (*72*). Second, the lipid diffusion space is unlikely to be homogeneous. Lipids bound directly at the protein surface

are motionally restricted, compared to bulk lipids, which could further hinder the diffusion process. Third, comparison with measured diffusion coefficients indicates that percolation analysis tends to overestimate the D^* values (*65*, *68*) leading to diffusion times that are lower than experimental values. Thus, the diffusion times calculated from percolation theory must be taken as a lower limit. These considerations point to the lifetime and the diffusion path for PQH_2, generated at PSIIα in a membrane with a random protein distribution and no differentiation between grana thylakoids and stroma lamella, being drastically increased by the obstruction of the lipid diffusion space. The times derived from percolation analysis tends to be higher than the intrinsic reaction time of the cytochrome bf complex, which is in the range of 3.3 to 5 ms (*58*, *73*). This reaction is known to be the rate-limiting step in electron transport (*74*, *75*). This implies that linear electron transport in a statistical membrane becomes diffusion limited. Under high light conditions, this situation would lead to an overreduction of the plastoquinone pool which can trigger acceptor side photoinhibition of photosystem II (*22*). Furthermore, a long lifetime for reduced PQ decreases the overall quantum efficiency of electron transport in low light, due to dissipation processes (*21*). In consequence, the PQ mediated electron transfer in a hypothetical membrane with a random protein distribution would be both dangerous and inefficient.

Comparison of the random protein distribution analyzed in this work with the native membrane makes it possible to speculate about the advantages that distinct architectural features of thylakoids might bring for the PQ diffusion process. One of the main differences is the differentiation between grana thylakoids and stroma lamellae. According to the thylakoid model of Albertsson (*23*), the core of the grana thylakoids contain only PSIIα, cyt.bf complexes and $LHCII_3$. This composition excludes complexes not involved in reactions with PQ (PSI, PSIIβ and the CFo-part of the ATPase) from the lipid space and increases the local concentration of reaction partners for plastoquinone (PSIIα, cyt.bf complex). Additionally, if one accepts the microdomain hypothesis, where (PSIIα-$LHCII_3$)-dimers and LHCII-trimers form temporarily enclosed lipid PQ-diffusion areas, further advantages are conceivable. If the microdomains build up a network-like structure, then a nearly protein free lipid area between the net-boundaries is likely. Two possibilities exist for the localization of cyt.bf dimers in these structures. The complex could be trapped, like plastoquinone, in a domain or could participate in the network structure. However, if we assume a distinct sealing of a microdomain, a reduced PQ released from a PSIIα "sees" only a small local lipid area. Thus, a fast unhindered redox contact to a cyt.bf complex located within this domain or at the domain boundary is possible. These considerations throw new light on the role of architectural features of the thylakoid membrane on the effectiveness of PQ-diffusion in this highly protein obstructed membrane. Enhancing the local concentrations of PSIIα and cyt.bf complexes by grana stacks and formation of nearly protein free lipid areas by microdomains could avoid a tortuous diffusion path. The "finding " of the right target protein would become much easier. Thus potential disadvantages connected with plastoquinone diffusion are minimized.

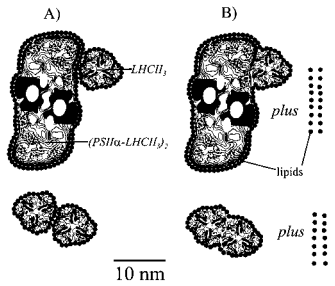

FIGURE 6: Models for the participation of boundary lipids in $(PSIIα\text{-}LHCII_3)_2 - LHCII_3$ (top) or $LHCII_3 - LHCII_3$ (bottom) associations. The protein shapes are taken from ref *4* for $(PSIIα\text{-}LHCII_3)_2$ and ref *2* for $LHCII_3$. The lipid molecular area was set to 0.54 nm^2 (see text). The docking sites for the $LHCII_3$ on the $(PSIIα\text{-}LHCII_3)_2$ supercomplex are taken from ref *9*. Panel A assumes that the contact zones between supercomplexes are spaced by lipids. Panel B proposes a lipid-free contact zone, leading to direct protein−protein interaction. The lipids depicted on the right-hand end are released from supercomplexes associations if direct protein−protein contact occurs. See text for further details.

Plastoquinone Concentration in the Lipid Bilayer. In the foregoing discussion, it was deduced that each chlorophyll molecule corresponds to a thylakoid membrane area of 1.71 ± 0.14 nm^2. The thickness of a lipid bilayer is 4.0 to 4.5 nm (4.3 ± 0.3 nm), as derived from analyzing the energetics of protein-membrane interactions (*76*). On the basis of these data, it can be calculated that each chlorophyll molecule is associated with a membrane volume of 7.35 ± 1.11 nm^3, equivalent to a concentration of 226 ± 34 mM. Furthermore, based on these values, the absolute plastoquinone concentration can be calculated. We estimate a PQ - pool size of 6.7 ± 0.4 (seven determinations) per photosystem II, from chlorophyll-*a* fluorescence induction experiments for our spinach preparation (not shown). This analysis includes the photoreducable plastoquinone pool only. In combination with the PSII concentration listed in Table 3, a value of 0.0190 ± 0.0025 PQ/chlorophyll molecule is determined (taking only PSIIα and β centers into account). From this value and the thylakoid volume corresponding to each chlorophyll derived above, we calculate a plastoquinone concentration of 4.3 ± 1.2 mM. It is important to note that about 70% of the thylakoid membrane is covered by proteins (see discussion above). It follows that the PQ concentration in the protein-free lipid space is 14 ± 7 mM, which is in agreement with a determination made by Blackwell and co-workers (*16*).

Boundary Lipids. Boundary lipids are relatively immobilized lipids, located in the first solvation shell of membrane complexes. In a first approximation, the number of these lipids can be deduced from the shape of these complexes (illustrated in Figure 6 for PSIIα and $LHCII_3$). Table 4 summarizes these numbers. An average molecular lipid area of 0.54 nm^2 is taken as a basis for these calculations, given a total number of 1.13 ± 0.08 boundary lipids per chlorophyll molecule (Table 4). Assuming that (i) no lipids are located *within* the supercomplexes and (ii) all supercomplexes are completely surrounded by lipids, 58 ± 10% of lipids contribute to the boundary lipid phase. The assumption that no lipids are located within complexes may be an oversimplification. No lipids are expected in the direct contact zones between proteins in supercomplexes. On the other hand, it is reasonable to assume that gaps or holes as, for example, seen between PSII in dimers, PSI and LHCI,

Table 4: Number and Concentration of Boundary Lipids of Integral Protein Supercomplexes[a]

	no. of boundary lipids per complex	conc of supercomplexes mmol/ mol of chl.	conc of boundary lipids mol/mol of chl.
$(PSII\alpha\text{-}LHC_3)_2$	168	1.09 ± 0.08	0.17 ± 0.01
$PSII\beta$[b]	114	0.66 ± 0.05	0.08 ± 0.01
$PSI\text{-}LHCI_8$	122	2.25 ± 0.17	0.27 ± 0.02
$LHCII_3$	58	9.05 ± 0.41	0.52 ± 0.02
$(cyt.bf)_2$	64	0.65 ± 0.03	0.04 ± 0.01
ATPase	52	0.95 ± 0.06	0.05 ± 0.01
total			1.13 ± 0.08

[a] The number of boundary lipids per complex is deduced from the protein shapes (see legend of Table 3). It is considered that boundary lipids should exist on both membrane sites (bilayer). [b] The number for $PSII\beta$ is derived from the $(PSII\alpha\text{-}LHCII_3)_2$ supercomplex assuming that $PSII\beta$ is a monomer without $LHCII_3$ bound. For the calculation of the concentration of boundary lipids (right column), the number of lipids per complex (left column) is multiplied by the concentration of supercomplexes (middle column).

or in LHCII trimers, are filled with boundary lipids. We estimate the following numbers of gap lipids from the structure of the supercomplexes (see legend in Table 4): 16 for $PSI\text{-}LHCI_8$, 12 for $(PSII\alpha\text{-}LHCII_3)_2$, 8 for $PSII\beta$, 2 for $LHCII_3$, and 18 for the CFo. However, the overall number of these "gap" lipids is relatively low. If these lipids are incorporated, the total fraction of boundary lipids only increases from 58% to about 64%. Recently, an alternative $PSII\alpha$ structure was postulated, where two additional LHCII-trimers and two CP24 proteins are attached to the $(PSIIa\text{-}LHCII_3)_2$ supercomplex (*77*). For this scenario, we calculate a boundary lipid fraction of about 54%. If we take the gap lipids into account, the fraction would be 60%.

The analysis of ESR spectra with spin labeled thylakoid lipids reveals two fractions of lipids. One fraction is composed of motionally restricted lipids while the other corresponds to free bulk lipids (*78*, *79*). It was found that the fraction of motionally restricted lipids strongly depends on the membrane protein-to-lipid ratio (*79*). To compare our data with the ESR analysis, we determined the protein content according to Markwell (*80*) as was done in the ESR experiments. On a weight basis, we determine a lipid/chlorophyll/protein ratio of 0.34:0.13:1. From these values, the ESR measurements would predict a fraction of motionally restricted MGDG of about 62% (*79*). As motionally restricted lipids detected by ESR analysis can be related to protein boundary lipids (*81*), there is a good agreement with our calculations.

Boundary Lipids in Higher Protein Associations. As stated above, we assume that all integral membrane supercomplexes are surrounded by boundary lipids. In the introduction, we summarized arguments for the existence of supercomplex aggregations, in particular between $(PSII\alpha\text{-}LHCII_3)_2$ and $LHCII_3$ in grana thylakoids. Two scenarios can be described for these associations: (i) the contact zones are lipid-containing areas where lipids prevent direct protein contact (Figure 6A); (ii) the contact zones between supercomplexes are lipid-free areas (direct protein−protein interactions; Figure 6B). From Figure 6, we can estimate the decrease in the number of boundary lipids for alternative B, assuming that all $LHCII_3$ docking sites on the $(PSII\alpha\text{-}LHCII_3)_2$ complex (*9*) are occupied by $LHCII_3$ and that two-thirds of the remaining $LHCII_3$ are connected. Given these assumptions, the fraction of boundary lipids decreases to $43 \pm 9\%$ (49% if gap lipids are taken into account). The true value is expected to be even lower, since postulated aggregations between $LHCII_3$ and a fraction of PSI complex (*12*, *13*) are not considered. However, a fraction of 43% is not in agreement with prediction from the ESR data (62%). We therefore conclude that the contact zones between supercomplexes in higher protein aggregation networks are spaced by lipids (Figure 6A). This view is supported by ESR measurements with spin-labeled PG, performed under different conditions. Neither protein phosphorylation nor destacking (which are known to disconnect a "mobile" LHCII fraction from PSII supercomplexes) increase the fraction of motionally restricted lipids (*82*). This indicates that weak associations between supercomplexes already contain lipids and do not bind them additionally upon dissociation.

From these considerations, a tentative picture for noncovalent protein−protein interactions in thylakoid membranes can be drawn: (i) Strong interactions exist between subunits in the multisubunit complexes of PSII, PSI, cyt.bf, and ATPase. (ii) Interactions of intermediate strength are responsible for supercomplex formation [$PSI\text{-}LHCI_8$, $(PSII\alpha\text{-}LHCII_3)_2$, $LHCII_3$, and $cyt.bf_2$]. It is expected that these associations contain only a few lipids, which could be important for the function of the protein complexes (*83*). (iii) Relatively weak interactions result in supercomplex associations, in particular among mobile $LHCII_3$ or between mobile $LHCII_3$ and $(PSII\alpha\text{-}LHCII_3)_2$. These supramolecular structures incorporate boundary lipids (Figure 6A) which is a qualitative difference to the former two interactions. The involvement of lipids could bring about flexibility and a more dynamic behavior of lateral supercomplex networks in thylakoids.

Lipid spaced supercomplex associations exclude the possibility of direct protein−protein interactions in the hydrophobic membrane phase. The question then arises, what forces are involved in this aggregation type? One possibility is that protein interactions occur between hydrophilic parts of supercomplexes. In this context, it is worth noting that all protein complexes extend a few nanometers over the lipid bilayer plane. Furthermore, the stroma-facing hydrophilic N-terminus of the LHCII seems to have a relatively high flexibility (*55*, *84*). Thus, it is conceivable that protein bridges in the aqueous phase above the lipid bilayer bring supercomplexes together.

Alternatively, it is possible that the aggregations are determined by lipid−lipid interactions. Horvarth and coworkers found that the association between PSII and $LHCII_3$ is a function of the hydrogenation status of lipids (*85*). They proposed that highly unsaturated fatty acids in the contact zones between LHCII and PSII are necessary for aggregation. Hydrogenation leads to a disconnection of LHCII from $PSII\alpha$ centers, resulting in $PSII\beta$ centers (*85*). Furthermore, Ivancich and co-workers (*86*) found an extremely immobilized boundary lipid fraction in PSII-enriched membrane preparations. About one-third of boundary lipids exchange much more slowly, or not at all, with bulk lipids, while the remaining fraction should have more rapid contact. It is possible that the former fraction represents boundary lipids located within supercomplex contact zones, while the latter fraction represents boundary lipids located outside these zones. From these

considerations, one can speculate that highly unsaturated, relatively immobilized lipids interact in supercomplex contact zones. From our data, we calculate that the lipid fraction located between supercomplexes is in the range of 23 and 28% of total boundary lipids. This range is lower than that determined in ref *86*, but it should be noted that these measurements were performed using PSII-enriched membranes, where supercomplex associations are expected to be more frequent. However, these points are speculative and further experiments are necessary to elucidate the driving forces for supercomplex aggregation.

In the same way as for the interaction hierarchy among protein complexes, a differentiation could also be made for lipids. "Bulk" lipids have the highest mobility. Boundary lipids not located between supercomplexes are motionally restricted but can exchange at a distinct rate with bulk lipids. Boundary lipids between supercomplexes could be extremely motionally restricted. Furthermore, a specialized lipid class could be involved in the catalytic function of supercomplexes (*83*).

ACKNOWLEDGMENT

The authors thank I. Volfson for kind help with the ATPase quantification, Dr. K. D. Mukherjee, Münster, for the help in lipid analysis, Dr. S. Krol, Münster, for the possibility to undertake surface-pressure area isotherms, and M. Lamborghini, Frankfurt a.M., for LHCII preparation, K. Topp and J. Scharte, Münster, for the support with the SDS-PAGE for LHCII quantification, and Dr. E. Weis for stimulating discussions. Furthermore, we thank Dr. D. Spiedel and Dr. G. Johnson for critical reading of the manuscript.

REFERENCES

1. Jansson, S. (1994) *Biochim. Biophys. Acta 1184*, 1−19.
2. Kühlbrandt, W., and Wang, D. N. (1991) *Nature 350*, 130−134.
3. Hope, A. B. (1993) *Biochim. Biophys. Acta 1143*, 1−22.
4. Hankamer, B., Barber, J., and Boekema, E. J. (1997) *Annu. Rev. Plant Physiol. Plant Mol. Biol. 48*, 641−671.
5. Boekema, E. J., Boonstra, A. F., Dekker, J. P., and Rögner, M. (1994) *J. Bioenerg. Biomembr. 26*, 17−29.
6. Boekema, E. J., and Lücken, V. (1996) In *Oxygenic Photosynthesis*: *The Light Reactions* (Ort, D. R., Yocum, C. F., Eds.) Kluwer, Dordrecht, pp 487−492.
7. Breyton, C. (2000) *J. Biol. Chem. 275*, 13195−13201.
8. Dekker, J. P., van Roon, H., and Boekema, E. J. (1999) *FEBS Lett. 449*, 211−214.
9. Boekema, E. J., van Roon, H., Calkoen, F., Bassi, R., and Dekker, J. P. (1999) *Biochemistry 38*, 2233−2239.
10. Krause, G. H., and Weis, E. (1991) *Annu. Rev. Plant Physiol. Plant Mol. Biol. 42*, 313−349.
11. Istokovics, A., Simidjiev, I., Lajkó, F., and Garab, G. (1997) *Photosynth. Res. 54*, 45−53.
12. Andreasson, E., and Albertsson, P.-A. (1993) *Biochim. Biophys. Acta 1141*, 175−182.
13. Svensson, P., Andreasson, E., and Albertsson, P.-A. (1991) *Biochim. Biophys. Acta 1060*, 45−50.
14. Joliot, P., Lavergne, J., and Béal, D. (1992) *Biochim. Biophys. Acta 1101*, 1−12.
15. Lavergne, J., Bouchaud, J.-P., and Joliot, P. (1992) *Biochim. Biophys. Acta 1101*, 13−22.
16. Blackwell, M., Gibas, C., Gygax, S., Roman, D., and Wagner, B. (1994) *Biochim. Biophys. Acta 1183*, 533−543.
17. Kirchhoff, H., Horstmann, S., Weis, E. (2000) *Biochim. Biophys. Acta 1459*, 148−168.
18. Joliot, P., and Joliot, A. (1992) *Biochim. Biophys. Acta 1102*, 53−61.
19. Staehelin, L. A. (1986) In *Encyclopedia of Plant Physiology Vol. 19* (Staehelin, L. A., and Arntzen, C. J., Eds.) Springer-Verlag, New York, pp 1−84.
20. Staehelin, L. A., and van der Staay, G. W. M. (1996) In *Oxygenic Photosynthesis: The Light Reactions* (Ort, D. R., and Yocum, C. F., Eds) Kluwer, Dordrecht, pp 11−30.
21. Lavergne, J., and Joliot, P. (1996) *Photosynth. Res. 48*, 127−138.
22. Barber, J., and Andersson, B. (1992) *Trends Biochem. Sci. 17*, 61−66.
23. Albertsson, P.-A. (1995) *Photosynth. Res. 46*, 141−149.
24. Anderson, J. M. (1992) *Photosynth. Res. 34*, 341−357.
25. Kramer, D. M., Joliot, A., Joliot, P., Crofts, A. R. (1994) *Biochim. Biophys. Acta 1184*, 251−262.
26. Diner, B. A., Petrouleas, V., and Wendoloski, J. J. (1991) *Physiol. Plant. 81*, 423−436.
27. Chapman, D. J., and Barber, J. (1986) *Biochim. Biophys. Acta 850*, 170−172.
28. Randall, P. J., and Bouma, D. (1973) *Plant Physiol. 52*, 229−232.
29. Porra, R. J., Thompson, W. A., and Kriedemann, P. E. (1989) *Biochim. Biophys. Acta 975*, 384−394.
30. Christie, W. W., and Dobson, G. (1999) *Lipid Technol. 11*, 64−66.
31. Roughan, P. G., and Batt, R. D. (1968) *Anal. Biochem. 22*, 74−88.
32. Bartlett, G. R. (1959) *J. Biol. Chem. 234*, 466−468.
33. Spittel, M. (2000) Ph.D. Thesis, University of Münster, Germany.
34. Metzger, S. U., Cramer, W. A., Whitmarsh, J. (1997) *Biochim. Biophys. Acta 1319*, 233−241.
35. Nelson, N., and Neumann, J. (1972) *J. Biol. Chem. 247*, 1819−1824.
36. Junge, W. (1976) In *Chemistry and Biochemistry of Plant Pigments Vol. 2* (Goodwin, T. W., Ed.) Academic Press, New York, pp 233−331.
37. McCauley, S. W., and Melis, A. (1986) *Biochim. Biophys. Acta 849*, 175−182.
38. Dekker, J. P., vanGorkom, H. J., Brok, M., Ouwehand, L. (1984) *Biochim. Biophys. Acta 764*, 301−309.
39. Ke, B. (1972) *Arch. Biochem. Biophys. 152*, 70−77.
40. Islam, K. (1987) *Biochem. Soc. Trans. 15*, 697−698.
41. Fiedler, H. R., Ponomarenko, S., von Gehlen, N., Strotmann, H. (1994) *Biochim. Biophys. Acta 1188*, 29−34.
42. Dittmer, J. C., and Lester, R. L. (1964) *J. Lipid Res. 5*, 126−127.
43. Quinn, P. J., and Williams, W. P. (1983) *Biochim. Biophys. Acta 737*, 223−266.
44. Murphy, D. J. (1986) *Biochim. Biophys. Acta 864*, 33−94.
45. Webb, M. S., and Green, B. R. (1991) *Biochim. Biophys. Acta 1060*, 133−158.
46. Joyard, J., Block, M. A., and Douce, R. (1991) *Eur. J. Biochem. 199*, 489−509.
47. Marsh, D. (1996) *Biochim. Biophys. Acta 1286*, 183−223.
48. Anderson, J. M., Chow, W. S., and Goodchild, D. J. (1988) *Aust. J. Plant. Physiol. 15*, 11−26.
49. Lee, W.-J., and Whitmarsh, J. (1989) *Plant Physiol. 89*, 932−940.
50. Burkey, K. O., and Wells, R. (1996) *Photosyn. Res. 50*, 149−158.
51. Melis, A. (1996) In *Oxygenic Photosynthesis: The Light Reactions* (Ort, D. R., and Yocum, C. F., Eds.) Kluwer, Dordrecht, pp 523−538.
52. Lavergne, J., and Briantais, J.-M. (1996) In *Oxygenic Photosynthesis: The Light Reactions* (Ort, D. R., and Yocum, C. F., Eds.) Kluwer, Dordrecht, pp 265−287.
53. Bassi, R., Marquardt, J., and Lavergne, J. (1995) *Eur. J. Biochem. 233*, 709−719.
54. Hsu, B.-D., and Lee, J.-Y. (1991) *Biochim. Biophys. Acta 1056*, 285−292.
55. Kühlbrandt, W., Wang, D. N., and Fujiyoshi, Y. (1994) *Nature 367*, 614−621.

56. Chain, R. K., and Malkin, P. (1991) *Photosynth. Res. 28*, 59−68.
57. Breyton, C., Tribet, C., Olive, J., Dubacq, J.-P., and Popot, J.-L. (1997) *J. Biol. Chem. 272*, 21892−21900.
58. Cramer, W. A., Soriano, G. M., Ponomarev, M., Huang, D., Zhang, S. E., Martinez, S. E., and Smith, J. L. (1996) *Annu. Rev. Plant Physiol. Plant Mol. Biol. 47*, 477−508.
59. Mörschel, E., and Staehelin, L. A. (1983) *J. Cell Biol. 97*, 301−310.
60. Xia, D., Yu, C.-A., Kim, H., Xia, J.-Z., Kachurin, A. M., Zhang, L., Yu, L., Deisenhofer, J. (1997) *Science 277*, 60−66.
61. Simpson, D. J. (1980) *Carlsberg Res. Commun. 45*, 201−210.
62. Demmig-Adams, B., Adams, W. W., III, Logan, B. A., Verhoeven A. S. (1995) *Aust. J. Plant Physiol. 22*, 249−260.
63. Grudzinski, W., Matula, M., Sielewiesiuk, J., Kernen, P., Krupa, Z., Gruszecki, W. I. (2001) *Biochim. Biophys. Acta 1503*, 291−302.
64. Horton, P., Ruban, A. V., Walters, R. G. (1996) *Annu. Rev. Plant Physiol. Plant Mol. Biol. 47*, 655−684.
65. Saxton, M. J. (1987) *Biophys. J. 52*, 989−997.
66. Saxton, M. J. (1989) *Biophys. J. 56*, 615−622.
67. Blackwell, M. F., Gounaris, K., Zara, S. J., and Barber, J. (1987) *Biophys. J. 51*, 735−744.
68. Blackwell, M. F., and Whitmarsh, J. (1990) *Biophys. J. 58*, 1259−1271.
69. Gupte, S., Wu, E. S., Hoechli, L., Jacobson, K., Sowers, A. E., Hackenbrock, C. R. (1984) *Proc. Natl. Acad. Sci. U.S.A. 81*, 2606−2610.
70. Drepper, F., Carlberg, I., Andersson, B., and Haehnel, W. (1993) *Biochemistry 32*, 11915−11922.
71. Drepper, F., Hippler, M., Nitschke, W., and Haehnel, W. (1996) *Biochemistry 35*, 1282−1295.
72. Marcus, R. A., and Sutin, N. (1985) *Biochim. Biophys. Acta 811*, 265−322.
73. Hauska, G., Schütz, M., and Büttner, M. (1996) In *Oxygenic Photosynthesis: The Light Reactions* (Ort, D. R., and Yocum, C. F., Eds.) Kluwer, Dordrecht, pp 377−398.
74. Stiehl, H. H., and Witt, H. T. (1969) *Z. Naturforsch. 24b*, 1588−1598.
75. Haehnel, W. (1984) *Annu. Rev. Plant Physiol. 35*, 659−693.
76. Yeates, T. O., Komiya, H., Rees, D. C., Allen, J. P., and Feher, G. (1987) *Proc. Natl. Acad. Sci. U.S.A. 84*, 6438−6442.
77. Eckardt N. A. (2001) *Plant Cell 13*, 1245−1248.
78. Li, G., Knowles, P. F., Murphy, D. J., Nishida, I., and Marsh, D. (1989) *Biochemistry 28*, 7446−7452.
79. Li, G., Knowles, P. F., Murphy, D. J., and Marsh, D. (1990) *Biochim. Biophys. Acta 1024*, 278−284.
80. Markwell, M. A. K., Haas, S. M., Tolbert, N. E., and Bieber, L. L. (1981) *Methods Enzymol. 72*, 296−303.
81. Williams, W. P. (1998) In *Lipids in Photosynthesis: Structure, Function and Genetics* (Siegenthaler, J.-P., and Murata, N., Eds.) Kluwer, Dordrecht, pp 103−118.
82. Li, G., Knowles, P. J., Murphy, D. J., and Marsh, D. (1990) *J. Biol. Chem. 265*, 16867−16872.
83. Siegenthaler, P.-A., and Trémolières, A. (1998) In *Lipids in Photosynthesis: Structure, Function and Genetics* (Siegenthaler, P.-A., and Murata, N., Eds.) Kluwer, Dordrecht, pp 145−173
84. Nilsson, A., Stys, D., Drakenberg, T., Spangfort, M. D., Forsén, S., and Allen, J. F. (1997) *J. Biol. Chem. 272*, 18350−18357.
85. Horváth, G., Melis, A., Hideg, E., Droppa, M., and Vigh, L. (1987) *Biochim. Biophys. Acta 891*, 68−74.
86. Ivancich, A., Horváth, L. I., Droppa, M., Horváth, G., and Farkas, T. (1994) *Biochim. Biophys. Acta 1196*, 51−56.
87. Boekema, E. J., Jensen, P. E., Schlodder, E., van Breemen, J. F. L., vanRoon, H., Scheller, H. V., and Dekker, J. P. (2001) *Biochemistry 40*, 1029−1036.
88. Gerken, S., Dekker, J. P., Schlodder, E., and Witt, H. T. (1989) *Biochim. Biophys. Acta 977*, 52−61.

BI011650Y